Constraint Effect in Tensile to Shear Type Transition

M. Mostafavi[a], D. J. Smith[b] and M.J. Pavier[c]

Department of Mechanical Engineering, Queen's Building,

University Walk, Bristol BS8 1TR, UK

[a]M.Mostafavi@Bristol.ac.uk, [b]David.Smith@Bristol.ac.uk, [c]Martyn.Pavier@Bristol.ac.uk

Keywords: Tensile type fracture, Shear type fracture, Mode I, Constraint

Abstract. There are two main fracture types in ductile materials: tensile type and shear type. It is believed that when the loading condition is predominantly tensile (mode I), tensile type fracture occurs and when it is mostly shear (mode II), shear type fracture occurs. Transition from tensile to shear type fracture is considered to occur at a certain proportion of mode I to mode II loading, irrespective of the level of constraint. However, this study reveals that the effects of constraint must be included because, depending on the level of constraint, transition may occur anywhere from mode I to mode II. A theoretical model of tensile to shear type fracture has been developed to include the effect of constraint. To provide experimental evidence for this theoretical model, the extreme case of mode I loading has been examined. It is shown that by reducing the constraint level to a low enough value, a tensile to shear type fracture transition takes place, even in mode I.

Introduction

For a ductile material, fracture typically occurs by void nucleation, growth and coalescence for mode I loading while fracture typically occurs by shear localisation for mode II loading. As the loading on the crack is changed from pure mode I to one with an increasing proportion of mode II, a transition from a tensile type fracture to a shear type fracture will usually occur. This transition is the subject of this paper.

The competition between tensile type and shear type failure mechanisms in cracked components has long been appreciated [1] and different terminologies have been used to describe these mechanisms. Conventionally, mode I has been used to describe tensile type failure and mode II to describe shear type fracture [2], but confusingly mode I loading does not necessarily result in mode I type failure, nor does mode II type loading result in mode II type failure. Knott [3] used the terms internal necking to describe the mechanism for tensile type failure and fast shear to describe that for shear type failure while Ayatollahi, Smith and Pavier [4] preferred the terms ductile tearing and shear localization. In the present work, the terms *tensile type* and *shear type* [5] will be used to differentiate between these two types of fracture.

The experimental test procedure to determine the transition from tensile type to shear type failure is almost identical in all studies. A cracked specimen is loaded under different modes of loading (from pure mode I to pure mode II) and the mode mixity at which the transition occurs is determined. The mode mixity at the transition is usually characterised by a mixity parameter M^P which is defined as:

$$M^P = \frac{2}{\pi}\tan^{-1}\left(\frac{K_I}{K_{II}}\right) \tag{1}$$

where M^P measures the contribution of mode II and mode I loading on a scale from zero to 1, where zero corresponds to pure mode II loading and 1 to pure mode I loading.

Aoki et al. [6] carried out fracture tests on A5083-O aluminium and found the transition occurred between $M^p = 0.31$ and $M^p = 0.55$. Bhattacharajee and Knott [7] used HY100 steel and found the transition point at $M^p = 0.6$. Amstutz et al. [8] found the transition in 2024-T3 aluminium when $M^p = 0.24$. Single edge notch (SEN) specimens were used by Smith and co-workers [9] to investigate the fracture properties of a rotor steel (3CrMo). They used a mixed mode fixture to achieve the complete range of mode mixities. They found that the fracture mechanism changed from transgranular cleavage to shear type failure at $M^p = 0.68$. They also reported that even when tensile type failure occurs, shear lips are observed at the edges of the specimens. This could be interpreted as a sign of a shear type failure at the edges of specimens due to a reduction in out of plane constraint.

Previous work in this area has attempted to explain the transition solely by considering the levels of mode I and mode II loading; however this has been found insufficient to explain all experimental observations. Indeed a shear type fracture may occur under pure mode I loading. The work described here included the effects of constraint on the tensile to shear type fracture transition with the result of much improved comparison with experiment. To this end, the *T*-stress is employed as the quantifying parameter for constraint and is incorporated into the available theoretical criteria for modelling this transition.

Theoretical Background

Chao and Liu [10], Li, Zhang, and Recho [11], Sutton et al. [12] and Ma et al. [13] have proposed theoretical models for tensile type to shear type fracture transition. In the remainder of this paper the focus will be on the Sutton et al. model (referred to as the SZBRD model) as the best agreement was found between this model and test results. This model can be interpreted as a competition between the maximum hydrostatic stress (for tensile type fracture) and the maximum equivalent von-Mises stress (for shear type fracture) near the crack tip. Based on the maximum hydrostatic stress criterion, tensile type fracture takes place when the maximum hydrostatic stress $\sigma_h^{\max}$ at the characteristic distance r_c in front of the crack reaches its critical value σ_h^c. The characteristic distance and critical stress are considered to be material properties. In a similar way, shear type fracture takes place when the maximum von-Mises stress $\sigma_e^{\max}$ reaches the critical shear stress σ_e^c at a radial distance from the crack tip equal to the characteristic distance. Therefore, if the maximum hydrostatic stress reaches its critical value while the von-Mises stress is less than its critical value, tensile type fracture occurs. Similarly, shear type fracture takes place if the maximum von-Mises stress attains its critical value and maximum hydrostatic stress is below its critical values. Hence, the transition from tensile type to shear type fracture may be predicted by the level of stress triaxiality T_f:

$T_{f,\max} > T_{f,c}$ for tensile type fracture

$T_{f,\max} < T_{f,c}$ for shear type fracture

where the stress triaxiality T_f is defined by

$$T_f = \frac{\sigma_h}{\sigma_e} \tag{2}$$

where σ_h is the hydrostatic stress

$$\sigma_h = \frac{\sigma_{\theta\theta} + \sigma_{rr} + \sigma_{zz}}{3} \tag{3}$$

and σ_e is the equivalent von Mises stress

$$\sigma_e = \frac{1}{\sqrt{2}}\sqrt{\left(\sigma_{rr} - \sigma_{\theta\theta}\right)^2 + \left(\sigma_{\theta\theta} - \sigma_{zz}\right)^2 + \left(\sigma_{zz} - \sigma_{rr}\right)^2 + 6\sigma_{r\theta}^2} \tag{4}$$

Smith et al. [14] showed that the *T*-stress is a simple yet accurate measure of constraint although only applicable to the case of small scale yielding. Therefore, incorporating the *T*-stress into expressions for the near crack tip hydrostatic and equivalent stresses will result in a modification to the tensile type to shear type failure transition model to include constraint. In order to do this the dimensionless characteristic distance α and the dimensionless *T*-stress B (also called the biaxiality ratio) are defined as:

$$\alpha = \sqrt{\frac{2r_c}{a}}, B = \frac{T\sqrt{\pi a}}{K_I} \tag{5}$$

Williams' asymptotic expansion for the stress distribution in the vicinity of the crack tip is represented as:

$$\begin{aligned}
\sigma_{rr}(r_c,\theta) &= \frac{K_I}{\sqrt{2\pi r_c}}\left\{\cos\frac{\theta}{2}\left[\left(1+\sin^2\frac{\theta}{2}\right)+\cot\left(\frac{\pi M^p}{2}\right)\left(\frac{3}{2}\sin\theta - 2\tan\frac{\theta}{2}\right)\right] + \alpha B\cos^2\theta\right\} \\
\sigma_{\theta\theta}(r_c,\theta) &= \frac{K_I}{\sqrt{2\pi r_c}}\left\{\cos\frac{\theta}{2}\left[\cos^2\frac{\theta}{2} - \frac{3}{2}\cot\left(\frac{\pi M^p}{2}\right)\sin\theta\right] + \alpha B\sin^2\theta\right\} \\
\sigma_{r\theta}(r_c,\theta) &= \frac{K_I}{2\sqrt{2\pi r_c}}\left\{\cos\frac{\theta}{2}\left[\sin\theta + \cot\left(\frac{\pi M^p}{2}\right)(3\cos\theta - 1)\right] - \alpha B\sin\theta\cos\theta\right\}
\end{aligned} \tag{6}$$

Usually the first singular term is used and the second, non-singular term (*T*-stress), is neglected. If however the second term is taken into account the critical mixity parameter at transition will depend on the level of constraint.

Fig. 1 illustrates the mixity parameter at transition using the modified SZBRD model for materials where $T_{f,c} = 0.75,\ 1.0$ and 1.4 for different values of αB from -0.6 to 0.4. The results of the original SZBRD model is indicated by T=0 on this graph. Fig. 1 depicts a strong constraint (αB) dependency on the mixity parameter at which transition occurs specially when αB is negative (i.e. low constraint). Also, it can be seen that the modified theory predicts shear type fracture in mode I if the constraint is low enough.

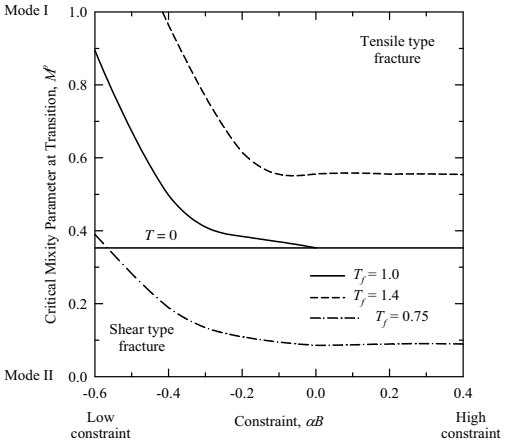

Fig. 1- Transition mixity parameter change in different constraint levels

Experiment

To verify the modified model, a set of 21 single edge crack bend specimens (Fig. 2) with different crack lengths have been tested. Aluminium 2024 has been selected as the test material because it shows limited plasticity upon fracture and can be considered to be in small scale yielding (SSY) conditions. In addition, this material shows a flat R-curve at room temperature which makes the fracture initiation detection straightforward.

Table 1- Details of the experiments

No.	Crack length a/W	Fracture toughness J_c (*MPa.mm*)	Maximum Triaxiality factor $T_{f,\max}$	Biaxiality ratio B
1	0.07	27.40	1.368	-0.392
2		30.65	1.380	
3		31.95	1.490	
4	0.12	38.98	1.563	-0.335
5		33.60	1.573	
6	0.13	46.29	1.646	-0.317
7	0.23	41.54	1.921	-0.202
8	0.25	41.99	1.923	
9		43.10	1.902	-0.182
10	0.35	51.55	2.080	-0.064
11		36.51	1.938	
12		53.48	2.092	
13	0.43	36.62	2.061	0.039
14		36.26	2.058	
15	0.45	40.49	2.092	0.061
16	0.53	40.52	2.156	0.196
17		33.31	2.069	0.173
18	0.55	33.66	2.073	
19	0.63	35.52	2.198	0.361
20		27.94	2.045	
21	0.67	26.31	1.982	0.296

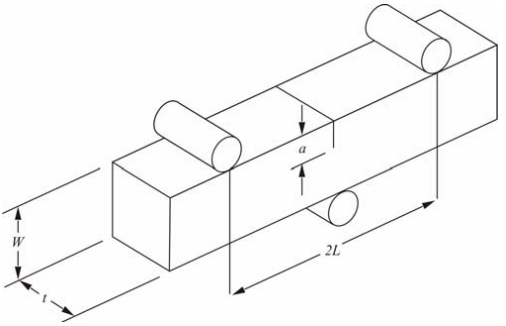

Fig. 2- Overview of the experiment configuration

Seven different crack lengths are selected corresponding to $a/W \approx 0.07, 0.12, 0.25, 0.35, 0.43, 0.53, 0.63$ (W=30mm, L=60mm, t=15mm). The difference in the crack length for the specimens provides different levels of constraint. Three specimens were used for each crack length to ensure the repeatability of the test. An EDM slot is introduced in each specimen followed by 2mm fatigue crack. Fatigue cracking is carried out in a three point bend configuration with maximum stress intensity factor less than one third of the fracture toughness.

Specimens were fractured using a 250kN servo hydraulic machine. To ensure that the loading can be considered to be static, the crosshead displacement rate was selected as low as 0.2 mm/min. The applied load and crosshead displacement were recorded using a computer at a rate of 10Hz. Details of the experimental results are reported in Table 1.

Finite Element Analyses

Three dimensional finite element analyses have been employed to obtain the fracture toughness of tested specimens and additional data that will allow predictions of the transition from tensile to shear type fracture. 20 node brick elements using the ABAQUS finite element code as shown in Fig. 3 are employed to simulate the fracture specimens. As shown in Fig. 3(b), concentrated collapsed elements were used as the first row of elements at the crack front. The size of the smallest element (at the crack tip) was 0.025mm to achieve at least 10 elements within the characteristic distance ($r_c = 500\mu m$). Symmetry allows just one quarter of the specimen to be modelled.

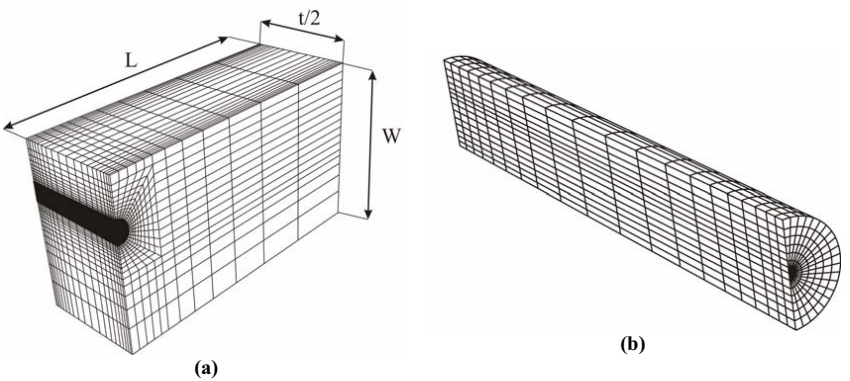

Fig. 3- Finite element model (a) overview (b) details of crack tip mesh

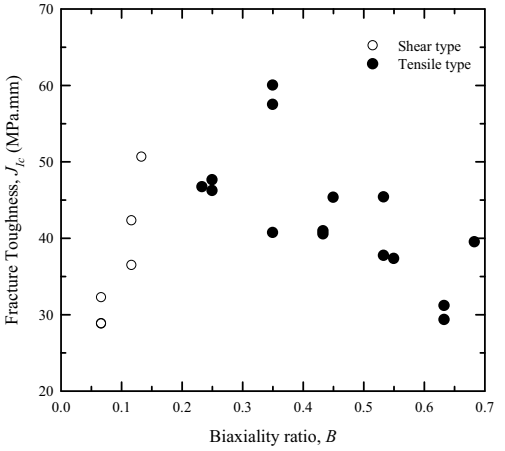

Fig. 4- Fracture toughness variation in specimens with different crack lengths

Elastic and elastic plastic analyses were performed to obtain the *T*-stress and fracture toughness. One simulation was performed using a contact technique to apply force to the specimen but no significant difference was observed between the results of this model and one where the force was distributed along a line. Therefore all the results reported here were obtained using a distributed force. Corresponding fracture toughness of the specimens is shown in Fig. 4.

Discussion

$\sigma_{h,\max}, \sigma_{e,\max}$ (Fig. 5) and $T_{f,\max}$ (Table 1) are extracted from the FE simulations, at the fracture load and at the characteristic distance. The maximum value was always observed in the middle of the specimen where crack initiation is believed to initiate [15]. Thus, despite the distribution through thickness of the specimens, single values of $\sigma_{h,\max}, \sigma_{e,\max}$ and $T_{f,\max}$ corresponding to the middle of plate are reported.

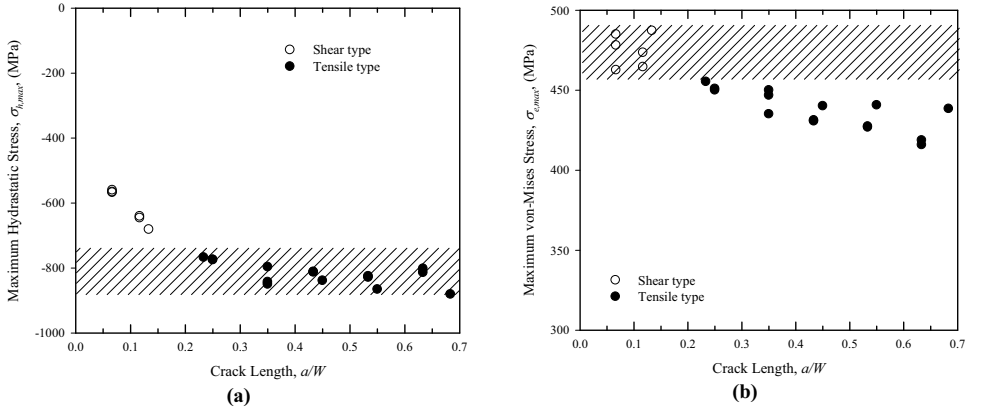

Fig. 5- Maximum (a) hydrostatic and (b) von Mises stresses in front of the crack tip at characteristic distance upon fracture in different specimens

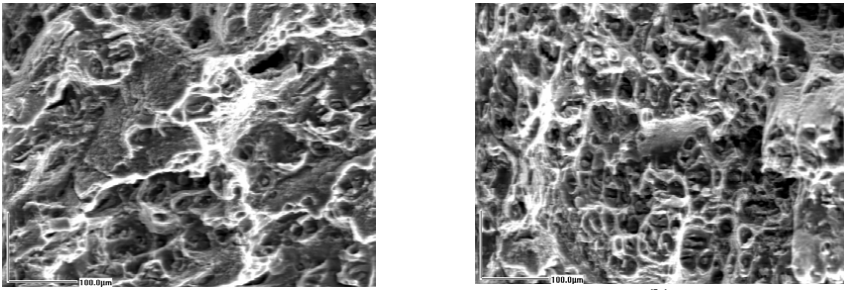

(a) (b)

Fig. 6- Fracture surface (a) $a/W = 0.07$ (b) $a/W = 0.63$

Whether tensile type or shear type fracture has occurred can be determined using a number of different techniques. The method used in this work is to check whether the maximum hydrostatic stress at fracture is constant as the crack length is varied. If it is, then the fracture type is held to be tensile type. Accordingly, using Fig. 5(a), the fracture type for the 4 longest cracks is found to be the tensile type. The rest of specimens showed shear type fracture (Fig. 5(b)). This is also confirmed by examining the fracture surface of the specimens using scanning electron microscope SEM pictures. Fractography reveals that large spherical voids can be observed in tensile type ductile fractures ($a/W > 0.25$) while parabolic small elongated voids may be seen in shear type fractures ($a/W < 0.25$). Fig. 6 shows the typical SEM pictures. Also an obvious drop in fracture toughness can be observed for cracks with length less than $a/W < 0.2$ which can be an indication of changing the fracture type from tensile to shear (Fig. 4).

Fig. 7 shows the comparison of the test results with the original and modified SZBRD models. The modified SZBRD model gives much better agreement. Experimental tests that show tensile type fracture (closed symbols) are above (to the right of) the transition curve and those that show shear type fracture (open symbol) are generally below (to the left of) the curve.

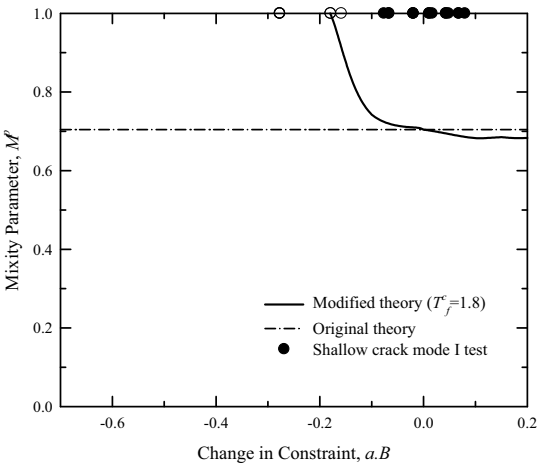

Fig. 7- Original and modified models compared with experimental values

Concluding Remarks

- It is found that shear type fracture can take place even in pure mode I if the constraint is low enough. This is confirmed by both FE analysis and experimental results.
- One of the available transition theories has been modified using non-singular term of stress in order to account for constraint effect. The modified theory showed improved consistency with experimental data

References

1. Clayton, J.Q. and J.F. Knott, *Observations of fibrous fracture modes in a prestrained low-alloy steel.* Metal Science, 1976. **10**(2): p. 63-71.
2. Hallback, N. and K.F. Nilsson, *Mixed-mode I-II fracture behaviour of an aluminium alloy.* Journal of Mechanics and Physics of Solids, 1997. **42**(9): p. 1345-1374.
3. Knott, J.F., *Micromechanis of fibrous crack extension in engineering alloys.* Metal Science, 1980. **August-September**: p. 327-336.
4. Ayatollahi, M.R., D.J. Smith and M.J. Pavier, *Effect of constraint on the initiation of ductile fracture in shear loading.* Key engineering materials, 2004. **261-263**: p. 183-188.
5. Tohgo, K. and H. Ishi, *Elastic-plastic fracture toughness test under mixed mode I-II loading.* Engineering fracture mechanics, 1992. **41**(4): p. 529-540.
6. Aoki, S., T. Kishimoto, T. Yoshida, M. Sakata and H.A. Richard, *Elastic-plastic fracture behavior of an aluminum alloy under mixed mode loading.* Journal of Mechanics and Physics of Solids, 1990. **38**(2): p. 195-213.
7. Bhattacharjee, D. and J.F. Knott, *Ductile fracture in HY100 steel under mixed mode I/mode II loading.* ACTA Metallurgica and Materials, 1994. **42**(5): p. 1747-1754.
8. Amstutz, B.E., M.A. Sutton, D. D.S. and J.C. Newman, *An experimental study of CTOD for model/mode II stable crack growth in thin 2024-T3 aluminum specimens*. ASTM STP 1256 on Fracture mechanics. 1995. 256-271.
9. Smith, D.J., M.R. Ayatollahi, J.C.W. Davenport and T.D. Swankie, *Mixed mode brittle and ductile fracture of a high strength rotor steel at room temperature.* International journal of fracture, 1998. **94**(3): p. 235-250.
10. Chao, Y.J. and S. Liu, *On the failure of cracks under mixed-mode loads.* International Journal of Fracture, 1997. **87**: p. 201-223.
11. Li, J., X.B. Zhang and N. Recho, *J-MP based criteria for bifurcation assessment of a crack in elastic-plastic materials under mixed mode I-II loading.* Engineering Fracture Mechanics, 2004. **71**: p. 329-343.
12. Sutton, M.A., W. Zhao, M.L. Boone, A.P. Reynolds and D.S. Dawicke, *Prediction of crack growth direction for mode I/II loading using small-scale yielding and void initiation/growth concepts.* International Journal of Fracture, 1997. **83**: p. 275-290.
13. Ma, F., X. Deng, M.A. Sutton and J.C. Newman, *A CTOD-based mixed mode fracture criterion, ASTM Special Technical Publication*. 1999. 86-110.
14. Smith, D.J., M.R. Ayatollahi and M.J. Pavier, *On the Consequences of T-stress in Elastic Brittle Fracture.* Proceedings of the Royal Society A, 2006. **462**: p. 2415-2437.
15. Anderson, T.L., *Fracture Mechanics - Fundamentals and Application*. 1995: CRC Press.